J. Fluid Mech. (1981), *vol.* 104, *pp.* 55–79
Printed in Great Britain

Large-eddy simulation of a passive scalar in isotropic turbulence

By M. ANTONOPOULOS-DOMIS
Department of Nuclear Engineering, Queen Mary College, Mile End Road, London E1 4NS

(Received 18 December 1979)

TEMTY, a code for large-eddy simulation of a passive scalar in isotropic turbulence, is developed and proved by successful simulation of experiment. The role of each term in the scalar equation and the concept of prefiltering the scalar equation is examined. The ratio of the exponents in the decay of velocity and temperature intensities is found to parametrize with the ratio λ_u/λ_θ, where λ_u, λ_θ are the velocity and temperature Taylor microscales respectively.

1. Introduction

Prediction of the mixing of a scalar in turbulent flows is of great importance. Yet, this is still extremely difficult owing to the limited understanding of the evolution of the velocity field and also of its coupling to the scalar field. Considerable theoretical and experimental research has been devoted to the behaviour of a passive scalar in homogeneous isotropic turbulence, but the state of knowledge of its structure and transport characteristics is unsatisfactory, even for this simplest case.

The aim of the present study is to demonstrate the feasibility of large-eddy simulation (LES) of such fields and use it to study the decay of a passive scalar (temperature fluctuations) in isotropic turbulence. In LES the flow-configuration-dependent 'large scales' (referred to as resolved scales) are explicitly computed, while the unresolved scales (also known as 'subgrid scales') which are expected to be universal (flow-configuration independent) are modelled. The theory of LES is discussed by Ferziger & Leslie (1979).

Since experimentation is always the basis confirming or rejecting any theoretical approach, the Yeh & Van Atta (1973) experiment is first simulated and the crucial parameter of the model determined. Then the concept of 'prefiltering' is tested for the scalar equations and finally the dependence of the scalar decay rate on the scalar and vector length scales is examined.

In what follows u_i ($i = 1, 2, 3$) are the fluctuating velocity components and θ the temperature fluctuations, and the summation convention is used, unless otherwise stated. The symbol $\langle c \rangle$ indicates the average of the variable c; the average is temporal if c is an experimental value, and is taken over the whole configuration space if c is obtained from the simulation.

0022-1120/81/4631-2890 $02.00

2. Experimental background

A number of experiments of decaying passive temperature fluctuations in approximately isotropic grid-generated turbulence have been carried out during the last decade to investigate the transport characteristics of a scalar in turbulence, e.g. Lin & Lin (1973), Mills *et al.* (1958), Sepri (1976), Warhaft & Lumley (1978), Yeh & Van Atta (1973). In these experiments the amplitude of θ was kept sufficiently small for buoyancy forces to be negligible, so that the temperature fluctuation was acting as a passive tracer. At a sufficient distance downstream from the grid, the scalar and velocity fields, viewed in a co-ordinate frame convected with the mean velocity U_0, approximate homogeneous isotropic conditions. Measurements were taken at a number of stations x/M, M being the grid spacing, and the kinetic energy was found to decay as

$$\tfrac{1}{2}\langle u_i^2\rangle \sim (x/M)^{-n}, \tag{2.1}$$

where n was a constant equal to $1{\cdot}3 \pm 0{\cdot}15$ for all experiments. On the other hand, although $\langle\theta^2\rangle$ was also found to decay as

$$\langle\theta^2\rangle \sim (x/M)^{-m}, \tag{2.2}$$

different experiments gave values of m ranging from 0·87 to 3·1. In view of the importance of the ratio $r = m/n$ in second-order modelling (see, for example, Newman, Launder & Lumley, 1980) and the expectation that the velocity time scale should be the controlling one, it is important to explain this variation of m and r. Warhaft & Lumley (1978) pointed out that there was an approximate trend for m to increase with increasing initial $\langle\theta^2\rangle$. It can be readily shown that, for these experiments, the influence of buoyancy is negligible; Warhaft & Lumley (1978) suggested that the amount of heat applied to the grid would influence the scales of the temperature fluctuations. They introduced a plane array of uniformly heated fine wires (the *mandoline*) downstream from the turbulence-producing unheated grid and thus succeeded in obtaining a control of the temperature scales independent of those of the velocity field. They found an almost linear relationship between m and the wavenumber k_θ at which the temperature spectrum peaked; since k_u, the wavenumber at which the velocity spectrum peaked, was constant, a linear relationship between m, r and k_θ/k_u might be implied. Herring & Newman (1979) were able to reproduce this trend using the test field model. Whilst this experiment provides a significant insight into turbulent mixing, a complete understanding of the scalar–vector coupling demands similar experiments, in which not only the scalar spectra-scales but also those of the velocity are varied. Such an exercise would obviously be costly and time-consuming.

With LES, once the simulation code is proven, one can change the input parameters at small additional cost; indeed we do so in the present study to investigate the dependence of m, r on length scales. Our LES code (TEMTY) has been tested by a successful simulation of the Yeh & Van Atta (1973) experiment.

3. Resolved field equations: subgrid models

The velocity field is described by the continuity and Navier–Stokes equations

$$\partial u_i/\partial x_i = 0, \tag{3.1}$$

$$\frac{\partial u_i}{\partial t} + \frac{\partial (u_i u_j)}{\partial x_j} = -\frac{\partial P_i}{\partial x_i} + \nu \nabla^2 u_i, \tag{3.2}$$

where $\langle u_i \rangle = 0$, p is the kinematic pressure and ν the kinematic viscosity. The temperature field is described by

$$\frac{\partial \theta}{\partial t} + \frac{\partial (\theta u_j)}{\partial x_j} = \nu_\theta \nabla^2 \theta, \tag{3.3}$$

where $\langle \theta \rangle = 0$, ν_θ is the thermal diffusivity and θ is sufficiently small for buoyancy forces to be negligible (whence their absence from (3.2)).

These equations describe fields which are continuous in both space and time. For numerical integration, the differential operators are approximated by finite-difference schemes, operating on discrete fields which are defined on a computational grid with mesh spacing h. The computation cannot resolve scales smaller than h; in other words we are resolving smoothed ('filtered') fields, the filtering being imposed by the discrete space configuration and the particular numerical scheme used. There have been two approaches to the definition of the resolved field. In the 'filter procedure' of Leonard (1974) a new field with filtered variables $\bar{f}$ is defined by convolution of each variable f of the original field with a filter function $G(\mathbf{x})$

$$\bar{f}(\mathbf{x}, t) = \int_{\text{all space}} G(\mathbf{x} - \mathbf{x}') f(\mathbf{x}', t)\, d\mathbf{x}'. \tag{3.4}$$

Among the filters used are the Gaussian:

$$G(\mathbf{x}) = \exp(-6\mathbf{x}^2/\Delta_A^2) \tag{3.5}$$

and the top-hat filter:

$$G(x) = \begin{cases} 1/\Delta_A^3 & \text{at} \quad |x - x_i'| < \tfrac{1}{2}\Delta_A \\ 0 & \text{otherwise,} \end{cases} \tag{3.6}$$

$$\Delta_A = nh, \quad n \geqslant 1,$$

where Δ_A is known as the filter width, and $\bar{f}(\mathbf{x}, t)$ is defined over all space. The so derived prefiltered equations are then approximated by difference equations and the computed variables are regarded as those of $\bar{f}(\mathbf{x}, t)$ at the points of the computational grid.

With the 'volume-balance' procedure of Schumann (1975) the resolvable variables $\bar{f}$ are defined only at the discrete grid points (x_1, x_2, x_3), as averages over grid volumes

$$\bar{f} = \frac{1}{h^3} \int_{x_1 - \frac{1}{2}h}^{x_1 + \frac{1}{2}h} \int_{x_2 - \frac{1}{2}h}^{x_2 + \frac{1}{2}h} \int_{x_3 - \frac{1}{2}h}^{x_3 + \frac{1}{2}h} dx_1\, dx_2\, dx_3 f(x_1, x_2, x_3). \tag{3.7}$$

Let f' be the unresolved part (also known as the subgrid scale term) of the variable f. Then after an application of either of the operations (3.4) or (3.7), which will be denoted by an overbar, and subsequent substitution of

$$f' = f - \bar{f} \tag{3.8}$$

the new equations read

$$\partial \bar{u}_i/\partial x_i = 0, \tag{3.9}$$

$$\frac{\partial \bar{u}_i}{\partial t} + \frac{\partial}{\partial x_j}(\overline{\bar{u}_i \bar{u}_j}) - \nu \frac{\partial^2}{\partial x_j^2}\bar{u}_i + \frac{\partial}{\partial x_j} R_{ij} = -\frac{\partial \bar{P}}{\partial x_i}, \tag{3.10}$$

$$\frac{\partial \bar{\theta}}{\partial t} + \frac{\partial}{\partial x_j}(\overline{\bar{\theta}\bar{u}_j}) + \frac{\partial}{\partial x_j} R_{\theta j} = \nu_\theta \frac{\partial}{\partial x_j}\bar{\theta}, \tag{3.11}$$

where the subgrid terms, which must be modelled in terms of the resolved variables, are defined by

$$R_{ij} = \overline{u_i' u_j'} + \overline{\bar{u}_i u_j'} + \overline{u_i' \bar{u}_j}, \tag{3.12}$$

$$R_{\theta j} = \overline{u_j' \theta'} + \overline{u_j' \bar{\theta}} + \overline{\bar{u}_j \theta'}. \tag{3.13}$$

In the volume balance procedure it is clear from (3.7) and (3.8) that:

$$\overline{\bar{u}_i \bar{u}_j} = \bar{u}_i \bar{u}_j, \tag{3.14}$$

$$\overline{\bar{\theta}\bar{u}_j} = \bar{\theta}\bar{u}_j, \tag{3.15}$$

$$\overline{\bar{u}_i u_j'} = \overline{u_i' \bar{u}_j} = \overline{u_j' \bar{\theta}} = \overline{\bar{u}_j \theta'} = 0. \tag{3.16}$$

With the prefiltering procedure (3.14)–(3.16) are, in general, not true as Leonard (1974) pointed out. For the top-hat and Gaussian filters, he has shown that

$$\left.\begin{aligned} \overline{\bar{u}_i \bar{u}_j} &= \bar{u}_i \bar{u}_j + \frac{\Delta_A^2}{24}\nabla^2(\bar{u}_i \bar{u}_j) + O(\Delta_A^4), \\ \overline{\bar{\theta}\bar{u}_j} &= \bar{\theta}\bar{u}_j + \frac{\Delta_A^2}{24}\nabla^2(\bar{\theta}\bar{u}_j) + O(\Delta_A^4). \end{aligned}\right\} \tag{3.17}$$

The second terms on the right-hand sides of (3.17) are known as the Leonard terms. Whilst $\partial(\bar{u}_i \bar{u}_j)/\partial x_j$, $\partial(\bar{\theta}\bar{u}_j)/\partial x_j$ conserve $\langle \bar{u}_i^2 \rangle$, $\langle \bar{\theta}^2 \rangle$, respectively, he predicted that the Leonard terms would provide a substantial contribution (more than 30 %) to the transfer of $\langle \bar{u}_i^2 \rangle$, $\langle \bar{\theta}^2 \rangle$ from the resolved to the subgrid scales, the rest being due to the subgrid stresses, R_{ij} and $R_{\theta j}$.

Mansour *et al.* (1979) used a Fourier transform method, instead of the Taylor expansion (3.17), to improve accuracy. With their method,

$$F(\overline{\bar{u}_i \bar{u}_j}) = F(G)\, F(\bar{u}_i \bar{u}_j), \tag{3.18}$$

where $F(y)$ denotes the Fourier transform of y. Given the fields $\bar{u}_i$, the right-hand side of (3.18) may be computed and $\overline{\bar{u}_i \bar{u}_j}$ obtained by inverse Fourier transformation. In both cases the prefiltering procedure is used and the only difference is in the accuracy of computation. In the present study the expressions (3.17) were used with the Leonard terms switchable to 'on' or 'off' so that the volume balance and the prefiltering procedures could be implemented in the same computer code. We may also note that the accuracy of (3.17) is sufficient ($O(\Delta_A^4)$), as can be clearly seen by comparison of the Kwak, Reynolds & Ferziger (1975) results, who used (3.17), with those of Mansour *et al.* (1979) who used (3.18) to simulate the same experiment. We may conclude that our findings, concerning the prefiltering procedure, are not restricted by the use of (3.17) rather than (3.18).

The prefiltering approach has been applied successfully (by Kwak *et al.* 1975) to simulate the near-isotropic velocity field of the Comte-Bellot & Corrsin (1971) experiment. A centred computational grid was used. It was found that inclusion of the Leonard term improved the simulated velocity spectra, but a filter width of $\Delta_A > h$ was necessary, the optimum being about $\Delta_A = 2h$. A detailed investigation of the two approaches and the relevant issues for the velocity field is given by Antonopoulos-Domis (1979). We briefly state here the main findings:

(*a*) On a staggered grid better results are obtained by omitting the Leonard term (i.e. using the volume balance procedure).

(*b*) Since the Leonard term is not necessary, scales down to the grid spacing h can be resolved.

(*c*) This term does not behave as predicted theoretically (Leonard 1974); on the contrary, its main effect is to backscatter energy from the highest resolved wavenumbers to smaller ones.

(*d*) Its contribution to energy transfer to the subgrid scales is negligible; this was also found to be the case for a centred grid (Kwak *et al.* 1975).

The subgrid scale (SGS) Reynolds stresses R_{ij}, which are responsible for the energy drain to the subgrid scales, are represented by an eddy viscosity model,

$$R_{ij} = -2\nu_u S_{ij} \tag{3.19}$$

and the Smagorinsky (1963) model for the eddy viscosity is used:

$$\nu_u = (c_u \Delta_A)^2 (2S_{ij}S_{ij})^{\frac{1}{2}}; \tag{3.20}$$

$$S_{ij} = \frac{1}{2}\left(\frac{\partial \overline{u}_i}{\partial x_j} + \frac{\partial \overline{u}_j}{\partial x_i}\right). \tag{3.21}$$

The determination of the model parameter c_u is discussed in §5. Note that with the volume balance procedure $\Delta_A = h$. The term $\partial R_{\theta j}/\partial x_j$, responsible for the drain of $\langle\theta^2\rangle$ to the subgrid scales, is here modelled in the same way; specifically

$$\frac{\partial}{\partial x_j} R_{\theta j} = -c_\theta \frac{\partial}{\partial x_j} \nu_u \frac{\partial \overline{\theta}}{\partial x_j}, \tag{3.22}$$

where the model parameter c_θ^{-1} can be thought of as an eddy Prandtl number.

We have already seen that the simulated fields are approximations to filtered versions of the 'real fields' whichever procedure is used. To distinguish between the volume balance and the filtering procedure we use the terms 'filtered' for variables derived with the former and 'prefiltered' for variables derived with the latter. The equations to be solved numerically now read

$$\frac{\partial \overline{u}_i}{\partial x_i} = 0, \tag{3.23}$$

$$\frac{\partial \overline{u}_i}{\partial t} = -\frac{\partial}{\partial x_j}\left(\overline{u}_i\overline{u}_j + F_{Lu}\frac{\Delta_A^2}{24}\nabla^2\overline{u}_i\overline{u}_j - 2\nu_u S_{ij}\right) + F_u \nu \nabla^2 \overline{u}_i - \frac{\partial \overline{p}}{\partial x_i} = H_i - \frac{\partial \overline{p}}{\partial x_i} = S_i, \tag{3.24}$$

$$\frac{\partial \overline{\theta}}{\partial t} = -\frac{\partial}{\partial x_j}\left(\overline{\theta}\,\overline{u}_j + F_{L\theta}\frac{\Delta_A^2}{24}\nabla^2\overline{\theta}\,\overline{u}_j - c_\theta \nu_u \frac{\partial \overline{\theta}}{\partial x_j}\right) + F_\theta \nu_\theta \nabla^2 \overline{\theta} = T, \tag{3.25}$$

where F_{Lu}, $F_{L\theta}$, F_u, F_θ are flags switching the relevant terms to 'on' or 'off'.

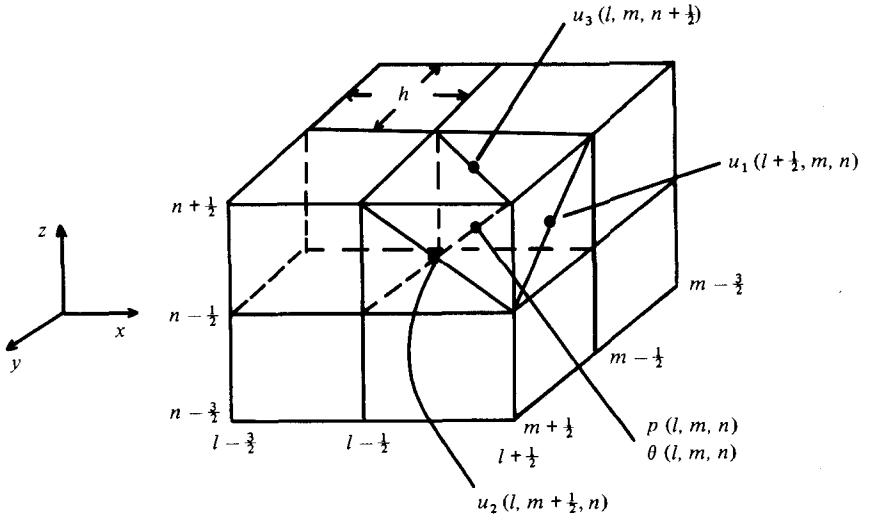

FIGURE 1. The staggered grid.

4. Numerical method

A staggered grid is used with a cubic mesh of width h (figure 1). The components of the velocity u are defined at the points $u_1(l+\frac{1}{2}, m, n)$, $u_2(l, m+\frac{1}{2}, n)$, $u_3(l, m, n+\frac{1}{2})$ and the pressure and temperature are defined at the points $p(l, m, n)$, $\theta(l, m, n)$. Details of the space-differencing schemes for the velocity field are given by Antonopoulos-Domis & Love (1978). Here we note that in the fourth-order version of TEMTY the terms $\partial(u_i u_j)/\partial x_j$ and $\partial p/\partial x_i$ are approximated to the fourth order, while all other terms are approximated to the second order.

Having the velocity field $u_i^{(n)}$ at time step n, the term $H_i^{(n)}$ (cf. equation (3.24)) is computed and the pressure is obtained by solving the Poisson equation

$$\frac{\partial^2}{\partial x_i} P^{(n)} = \frac{\partial H_i^{(n)}}{\partial x_i} \tag{4.1}$$

with fast-Fourier-transform techniques. The term $S_i^{(n)}$ is then computed. Similarly the right-hand side $T^{(n)}$ of (3.25) is obtained from the fields $\theta^{(n)}$, $u_i^{(n)}$. Statistics of the fields are computed every NLEAP time steps. On the first time step and every NLEAP time step the Euler method of time differencing:

$$u_i^{(n+1)} = u_i^{(n)} + \Delta t S_i^{(n)} + O(\Delta t^2), \tag{4.2}$$

$$\theta^{(n+1)} = \theta^{(n)} + \Delta t T^{(n)} + O(\Delta t^2) \tag{4.3}$$

is used. For every other time step the Adams–Bashforth method

$$u_i^{(n+1)} = u_i^{(n)} + \Delta t[\tfrac{3}{2} S_i^{(n)} - \tfrac{1}{2} S_i^{(n-1)}] + O(\Delta t^3), \tag{4.4}$$

$$\theta^{(n+1)} = \theta^{(n)} + \Delta t[\tfrac{3}{2} T^{(n)} - \tfrac{1}{2} T^{(n-1)}] + O(\Delta t^2) \tag{4.5}$$

is used. The space-differencing schemes approximating the differential operators of (3.25) are as follows.

For the homogeneous isotropic turbulence periodic boundary conditions are imposed on the calculational box; and

$$\int_{\text{volume of box}} dV \frac{\partial u_j \theta}{\partial x_j} = 0, \tag{4.6}$$

$$\int_{\text{volume of box}} dV \theta \frac{\partial \theta u_j}{\partial x_j} = 0. \tag{4.7}$$

The numerical scheme for the convective term has therefore to satisfy the conditions

$$\sum_{l,m,n=1}^{N} \frac{\delta}{\delta x_j} u_j(l,m,n)\,\theta(l,m,n) = 0, \tag{4.8}$$

$$\sum_{l,m,n=1}^{N} \theta(l,m,n) \frac{\delta}{\delta x_j} u_j(l,m,n)\,\theta(l,m,n) = 0. \tag{4.9}$$

Two schemes were used; one was second- and the other fourth-order accurate. The temperature and velocity components are not defined at the same grid points, and the interpolation operators a_j, $a_{j,(3)}$ have to be used, where

$$a_1 f(l,m,n) = \tfrac{1}{2}[f(l+\tfrac{1}{2},m,n)+f(l-\tfrac{1}{2},m,n)], \tag{4.10}$$

$$a_{1,(3)} f(l,m,n) = \tfrac{1}{2}[f(l+\tfrac{3}{2},m,n)+f(l-\tfrac{3}{2},m,n)] \tag{4.11}$$

with similar relations for a_2, a_3, $a_{1,(3)}$, $a_{2,(3)}$, $a_{3,(3)}$. The second-order finite-difference scheme satisfying (4.8) and (4.9) and giving the convective term at the points (l,m,n) is

$$\frac{\partial \theta u_j}{\partial x_j} = \frac{\delta \theta u_j}{\delta x_j}\bigg|_{l,m,n} + O(h^2) = \delta_j[u_j(a_j\theta)] + O(h^2), \tag{4.12}$$

while the fourth-order scheme is

$$\frac{\partial \theta u_j}{\partial x_j} \overset{\Delta}{=} \frac{\delta \theta u_j}{\delta x_j}\bigg|_{l,m,n} + O(h^4) = \tfrac{1}{8}\{9\delta_j[u_j(a_j\theta)] - \delta_{j(3)}[u_j(a_{j(3)}\theta)]\} + O(h^4). \tag{4.13}$$

Here the difference operators δ_j, $\delta_{j(3)}$ are defined by

$$\delta_1 f(l,m,n) = \frac{1}{h}[f(l+\tfrac{1}{2},m,n) - f(l-\tfrac{1}{2},m,n)] \tag{4.14}$$

and

$$\delta_{1(3)} f(l,m,n) = \frac{1}{3h}[f(l+\tfrac{3}{2},m,n) - f(l-\tfrac{3}{2},m,n)] \tag{4.15}$$

with similar relations for the δ_2, δ_3, $\delta_{2(3)}$, $\delta_{3(3)}$. The eddy viscosity is defined at the points (l,m,n); the scheme giving the subgrid terms at (l,m,n) is

$$\frac{\partial}{\partial x_j}\left(\nu_u \frac{\partial \theta}{\partial x_j}\right) \overset{\Delta}{=} \delta_j\{[a_j \nu_u(j+\tfrac{1}{2})]\delta_j\,\theta\} + O(h^2). \tag{4.16}$$

The second-order central-difference scheme is used for the term $\partial^2\theta/\partial x_j^2$, as well as for the Leonard term.

The initial velocity field $u_i(\mathbf{x})$ is derived from a random Gaussian field with zero mean, obeying the continuity condition $\partial \overline{u}_i/\partial x_i = 0$; any prescribed three-dimensional

spectrum can be imposed. The random, Gaussian initial temperature field is formed in the same way.

5. Results and discussion

5.1. *Model parameters: simulation of the Yeh & Van Atta experiment*

There are two model parameters to be determined, C_u and C_θ. C_u is known to depend on a subgrid-scale Reynolds number R_{SGS} (McMillan & Ferziger 1979; Ferziger & Leslie 1979). At low R_{SGS} it can be determined without recourse to experiment, by reference to fields generated by direct simulation of homogeneous isotropic turbulence as the 'original fields' to be simulated (McMillan & Ferziger 1979). Alternatively it can be determined by fixing Cu to match the simulated kinetic energy decay with that of a particular experiment (Kwak *et al.* 1975). Values of Cu obtained by the two methods using the prefiltering approach were found to be in good agreement with each other but in fair agreement only with theoretical predictions (Ferziger & Leslie 1979). Simulation of the velocity fields of the Comte-Bellot & Corrsin (1971) and the Yeh & Van Atta (1973) experiments using the volume balance procedure by Antonopoulos-Domis (1979) gave values of Cu in excellent agreement with the theoretical predictions of Lilly (1966).

Similarly the model parameter C_θ can be determined by either of the two methods. Here it is determined by matching to the $\langle\theta^2\rangle$ decay of the Yeh & Van Atta (1973) experiment; the advantage is in the confidence inherent in the experimental matching, the disadvantage in the possible restriction of the C_θ so determined to the neighbourhood at the Reynolds and Prandtl numbers of the experiment. In the latter the (passive) temperature fluctuations were generated by heating the turbulence-producing grid and the characteristic parameters were:

grid spacing,	$M = 40$ mm;
free-stream air speed,	$U_0 = 4{\cdot}06$ m s^{-1};
temperature intensity at $x/m = 35$,	$\langle\theta^2\rangle = 0{\cdot}2776$ °C;
Taylor velocity microscale at $x/m = 35$,	$\lambda_u = 6{\cdot}25$ mm, $R_\lambda = u_1\lambda_u/\nu = 35{\cdot}2$;
Kolmogorov velocity microscale,	$\eta_u = (\nu^3/\epsilon)^{\frac{1}{4}} = 0{\cdot}534$ mm;
Kolmogorov temperature microscale,	$\eta_\theta = (\nu_\theta^3/\epsilon)^{\frac{1}{4}} = 0{\cdot}679$ mm.

From (5.1) it is evident that the three-dimensional filtered spectra $\bar{E}(k)$ can be obtained from the raw experimental as

$$\bar{E}_{\exp}(k) = E_{\exp}(k).|G(k)|^2, \tag{5.1}$$

where the transform $G(k)$ of the Gaussian filter (3.5) is

$$G(k) = \exp(-k^2\Delta_A^2/24) \tag{5.2}$$

while the transform of the top-hat filter is

$$G(\mathbf{k}) = B(k_1\Delta_A)\,B(k_2\Delta_A)\,B(k_3\Delta_A), \tag{5.3}$$

$$B(\xi) = \sin(\tfrac{1}{2}\xi)/(\tfrac{1}{2}\xi). \tag{5.4}$$

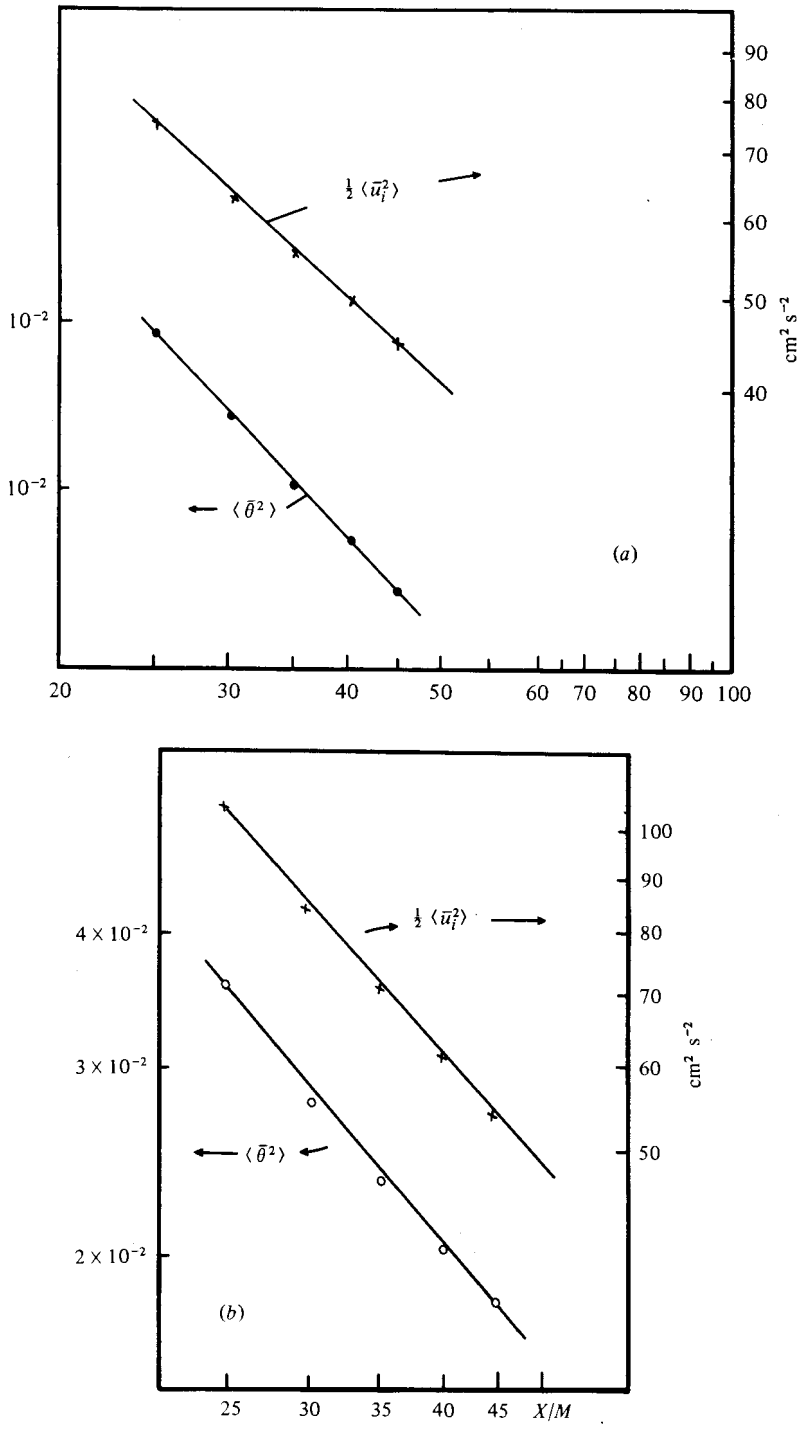

FIGURE 2. Decay of $\frac{1}{2}\langle\bar{u}_i^2\rangle$ and $\langle\bar{\theta}^2\rangle$, (*a*) 16^3 runs, $h = 1{\cdot}5$ cm, (*b*) 32^3 runs. Leonard term not included. $C_u = 0{\cdot}23$, $C_\theta = 2{\cdot}0$, ——, filtered experimental. Simulation: × × ×, $\frac{1}{2}\langle\bar{u}_i^2\rangle$; ○ ○ ○, $\langle\bar{\theta}^2\rangle$.

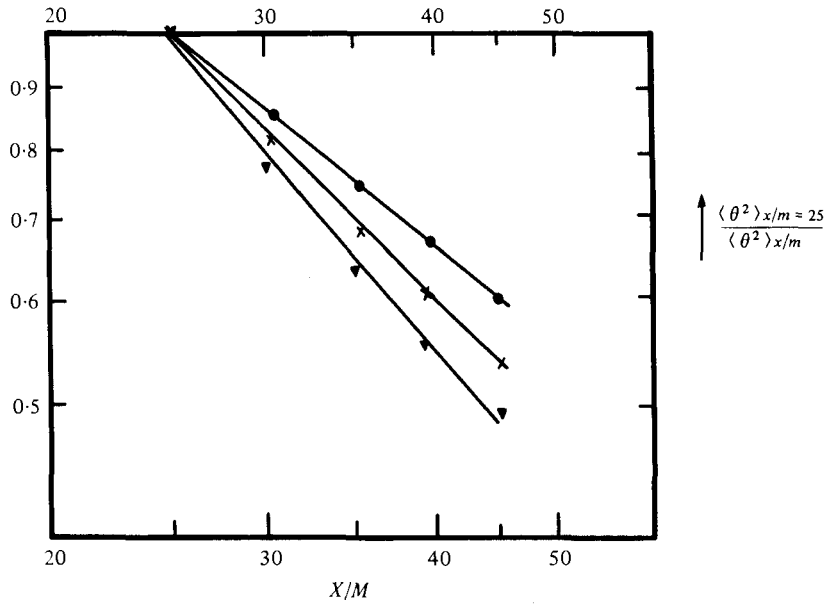

FIGURE 3. Sensitivity of $\langle\bar{\theta}^2\rangle$ decay on C_θ. ○, $C_\theta = 1{\cdot}5$; ×, $C_\theta = 2{\cdot}0$; ▽, $C_\theta = 2{\cdot}5$.

It can readily be seen from (3.7) that the filter inherent in the volume balance procedure is the top-hat (5.3) with $\Delta_A = h$. It should also be noted that, up to the maximum wave number ($k_{\max} = \pi\sqrt{3}/h$) that can be resolved, the filtering effects of (5.3) and (5.5) are almost identical; therefore their difference is, for all practical purposes, conceptual rather than real (Antonopoulos-Domis 1979).

The filtered kinetic energy $\frac{1}{2}\langle\bar{u}_i^2\rangle$ and the temperature variance $\langle\bar{\theta}^2\rangle$ at various stations x/M are obtained from the experimental three-dimensional spectra:

$$\tfrac{1}{2}\langle\bar{u}_i^2\rangle_{\exp} = \int_0^\alpha \bar{E}_{u\exp}(k)\,dk, \tag{5.5}$$

$$\langle\bar{\theta}^2\rangle_{\exp} = \int_0^\alpha \bar{E}_{\theta\exp}(k)\,dk. \tag{5.6}$$

In view of the finding for the velocity field (see §3) the velocity Leonard term was switched 'off' ($F_{Lu} = 0$ in (3.24)) for all the runs of the present study.

The contribution of the molecular viscosity term to the total energy dissipation is small for coarse meshes, but it becomes non-negligible as h is made smaller; switching off this term affects the value of Cu (Antonopoulos-Domis 1979). For the coarse meshes to which we are at present limited, this effect can be neglected and the difference lumped into the subgrid term. This was done for the runs reported in this section; the effect of doing so is discussed in §3.2.

The three-dimensional filtered experimental spectra at station $x/M = 25$ were imposed on the initial fields of both velocity and temperature. A small mesh size h is desirable for capturing as much as possible of the high wavenumber part of the spectrum ($k_{\max} = \pi\sqrt{3}/h$). On the other hand, h must be large enough to include the

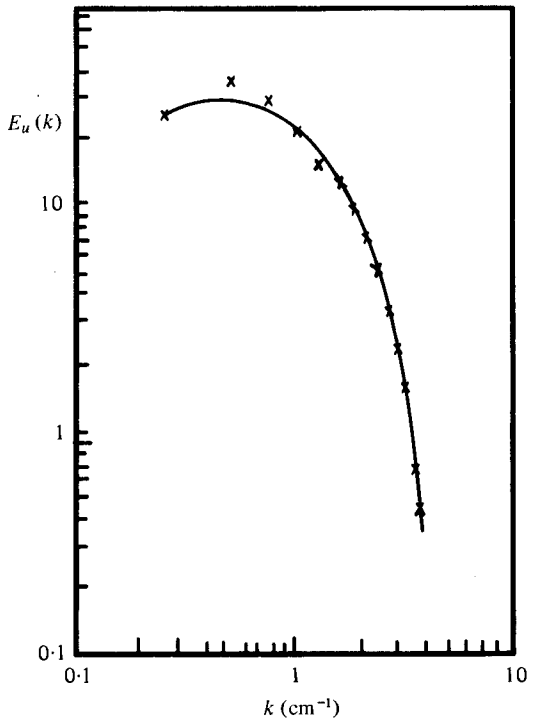

FIGURE 4. Three-dimensional velocity spectra, 16^3 runs, $h = 1{\cdot}5$ cm. No Leonard term, ——, filtered experimental ($X/M = 46{\cdot}6$); × × ×, simulation.

important part of the large scales ($k_{\min} = \pi\sqrt{3}/hN$, N = number of grid points in any one direction). For the simulation of the present experiment it was chosen to be

$$h = 15 \text{ mm} \quad \text{for } 16^3 \text{ runs},$$
$$h = 10 \text{ mm} \quad \text{for } 32^3 \text{ runs}.$$

The value of Cu matching the experimental $\langle \overline{u}_i^2 \rangle$ decay was found to be the same as that for the Comte-Bellot & Corrsin (1971) experiment in which $Re_\lambda = 71{\cdot}6$, namely

$$Cu = 0{\cdot}23. \tag{5.7}$$

In figure 2(a) the simulated and filtered experimental decay of $\langle \overline{u}_i^2 \rangle$ are compared for the 16^3 runs; the same comparison for the 32^3 grid-box runs is given in figure 2(b). It will be noted that Cu is independent of the size of the mesh spacing for $Fu = 0$. For the coarse meshes to which we are limited, the dissipation of $\langle \overline{\theta}^2 \rangle$ by the thermal diffusivity term at scales larger than h is a small fraction of the total drain of $\langle \overline{\theta}^2 \rangle$ to the subgrid scales. For the runs of this section this term was switched off ($F_\theta = 0$), which is equivalent to lumping the difference into the subgrid term; its effect is investigated in the next section. The temperature Leonard term was also switched off ($F_{L\theta} = 0$) and the value of C_θ matching the filtered experimental decay of $\langle \overline{\theta}^2 \rangle$ was found (figures 2a, b) to be

$$C_\theta = 2{\cdot}0. \tag{5.8}$$

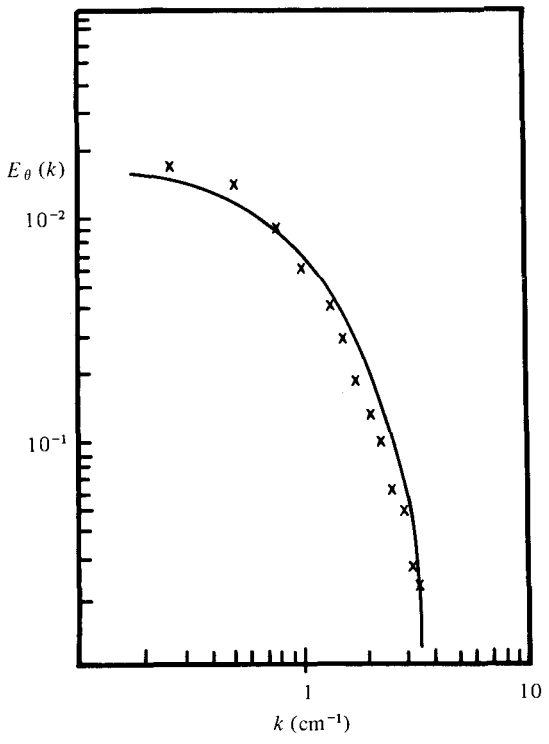

FIGURE 5. Three-dimensional temperature spectra, 16^3 runs, $h = 1{\cdot}5$ cm. No Leonard term, $C_\theta = 2{\cdot}0$, $X/M = 46{\cdot}5$. ——, filtered experimental; × × ×, simulation.

It may be shown by an easy extension of Lilly's analysis that, if there is a well-developed inertial range,

$$C_\theta = (Ko/Ba), \tag{5.9}$$

where Ko is the Kolmogorov constant and Ba is the corresponding constant for the scalar field, defined by

$$E_{\text{scalar}}(k) = Ba\,\chi\epsilon^{-\frac{1}{3}}k^{-\frac{5}{3}} \tag{5.10}$$

χ being the scalar and ϵ the kinetic energy dissipation rates respectively. A literature search by Quarini (1977) shows that experimental values for Ko agree quite well ($Ko \simeq 1{\cdot}5$). The majority of the experimental values for Ba agree quite well, giving a mean $Ba \simeq 0{\cdot}63$, with the exception of two experiments where Ba is reported to be two to three times larger; including the latter an arithmetic mean of $Ba \simeq 0{\cdot}83$ is obtained. Thus equation (5.9) would give $C_\theta = 1{\cdot}8$ to $2{\cdot}38$ which is in good agreement with (5.8), considering the scatter of the Ba values. In figure 3, the sensitivity of the simulated decay of $\langle\overline{\theta}^2\rangle$ to C_θ is shown.

The three-dimensional spectra of velocity and temperature fluctuations for 16^3 runs and 32^3 runs are shown in figures 4–7. The agreement with the filtered experimental spectra ranges from good to excellent, and this shows that:

(*a*) The LES code TEMTY is capable of predicting the evolution of the vector and scalar field statistics.

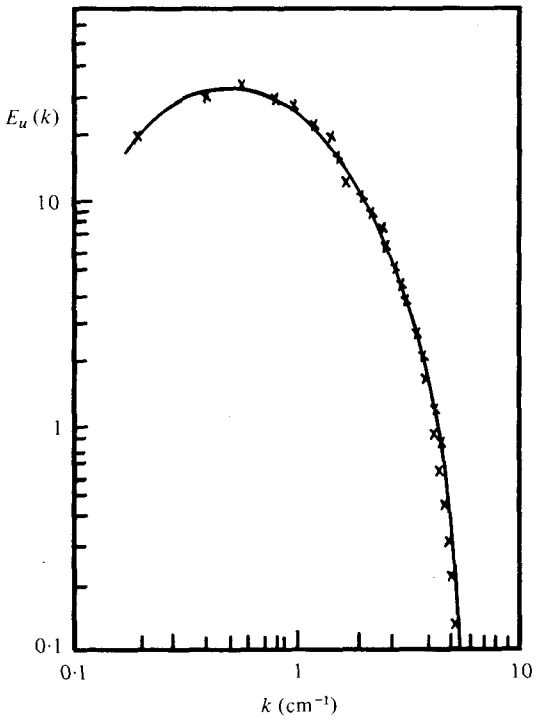

FIGURE 6. Three-dimensional velocity spectra, 32^3 runs, $h = 1$ cm. No Leonard term, $C_u = 0{\cdot}23$, $X/M = 46{\cdot}5$. ——, filtered experimental; × × ×, simulation.

(*b*) The Leonard term, hence prefiltering of the scalar equations, is not necessary, at least for a staggered grid; this conclusion is consistent with the findings for the velocity field. Its significance is that scales down to the mesh spacing h can be resolved for both the velocity and the scalar fields.

(*c*) The subgrid scale term (3.13) is successfully modelled by the eddy diffusivity model (3.22) in the case of isotropic flows.

(*d*) The spectral agreement between simulation and experiment for both 16^3 and 32^3 runs confirms that the model parameter C_θ is independent of the mesh size, if the effects of viscosity and diffusivity are lumped into the respective subgrid terms.

5.2. *Role of each term of the scalar equation – prefiltering*

To investigate the role of each term in the temperature equation 16^3 runs ($h = 1{\cdot}5$ cm) were used and the velocity Leonard term was switched off ($F_{Lu} = 0$). The initial fields were those of the Yeh & Van Atta experiment.

First the thermal diffusivity and the temperature Leonard terms were switched off ($F_{L\theta} = F_\theta = 0$) in (3.25) and the model parameter C_θ was set equal to 0. We were then following the evolution of a $\overline{\theta}$ which obeys

$$\frac{\partial \overline{\theta}}{\partial t} + \frac{\partial(\overline{\theta}\overline{u}_j)}{\partial x_j} = 0, \tag{5.11}$$

and this is a direct simulation without subgrid drain. The spectral results are shown in figure 8.

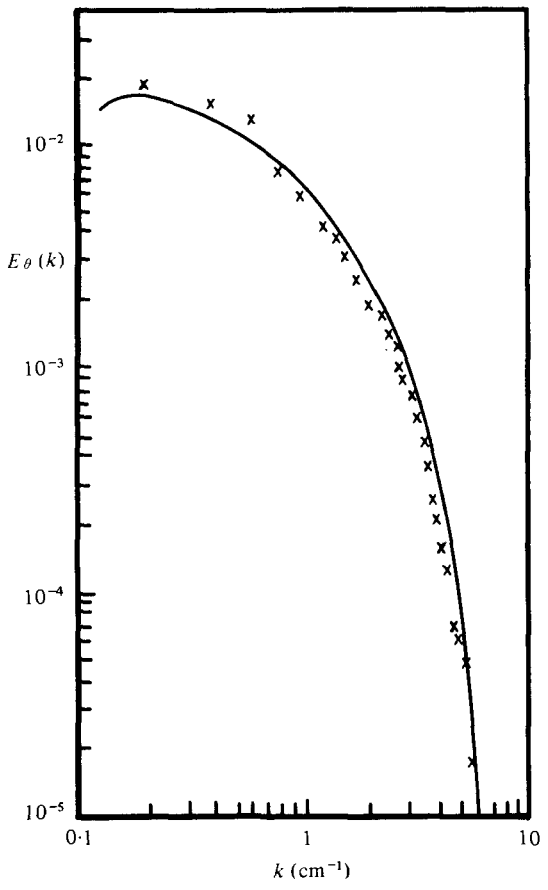

FIGURE 7. Three-dimensional temperature spectra, 32^3 runs, $h = 1$ cm. No Leonard terms, $C_\theta = 2{\cdot}0$, $X/M = 46{\cdot}5$. ——, filtered experimental; × × ×, simulation.

The variance $\langle\overline{\theta}^2\rangle$ was constant, for all time steps (since the numerical scheme for $\partial(\overline{\theta}\overline{u}_j)/\partial x_j$ is conserving $\langle\overline{\theta}^2\rangle$ and the effect of the convective term was, as it should be, to transfer $\langle\overline{\theta}^2\rangle$ from low wavenumbers to high ones, with a sharp cut-off at the maximum resolvable k. Comparing figure 8 with figure 5, it is clear that the subgrid term is dissipating $\langle\overline{\theta}^2\rangle$ mainly from the high wavenumber part of the resolved scales to the unresolved scales, which is exactly what it is meant to do.

The calculation was then repeated with exactly the same initial conditions and the Leonard term included ($F_{L\theta} = 1$), $\Delta_A = h$ and $C_\theta = 0$; we were then following the evolution of a θ satisfying

$$\frac{\partial\overline{\theta}}{\partial t} + \frac{\partial}{\partial x_j}\overline{\theta}\overline{u}_j + \frac{h^2}{24}\nabla^2\overline{\theta}\overline{u}_j = 0. \tag{5.12}$$

It was found that the Leonard term contribution to the transfer of $\langle\overline{\theta}^2\rangle$ to subgrid scales was negligible; this result, consistent with the findings for the velocity field, does not verify Leonard's (1974) predictions of the role of 'his' term. The spectral results are shown in figure 9; subtracting the spectral values of the field satisfying (5.12) from those of the (5.13) field (both at the 32nd time step), we get the effect of the

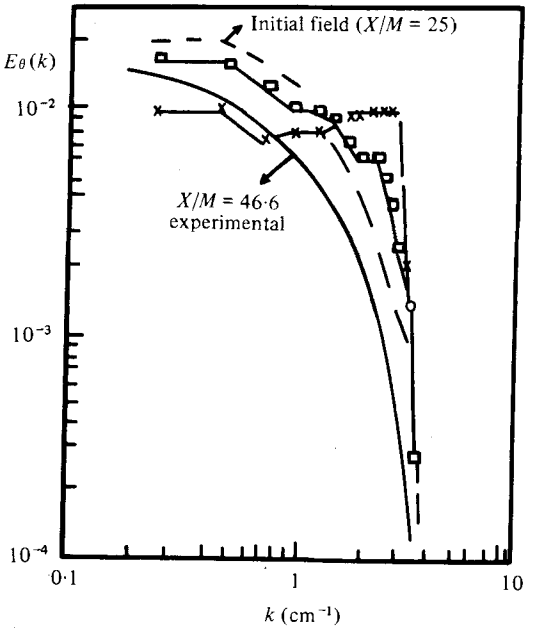

FIGURE 8. Role of convective term, 16^3 runs, h = 1·5 cm. Leonard, subgrid and diffusivity terms not included. □, 16 time steps (X/M = 45); ×, 32 time steps (X/M = 65).

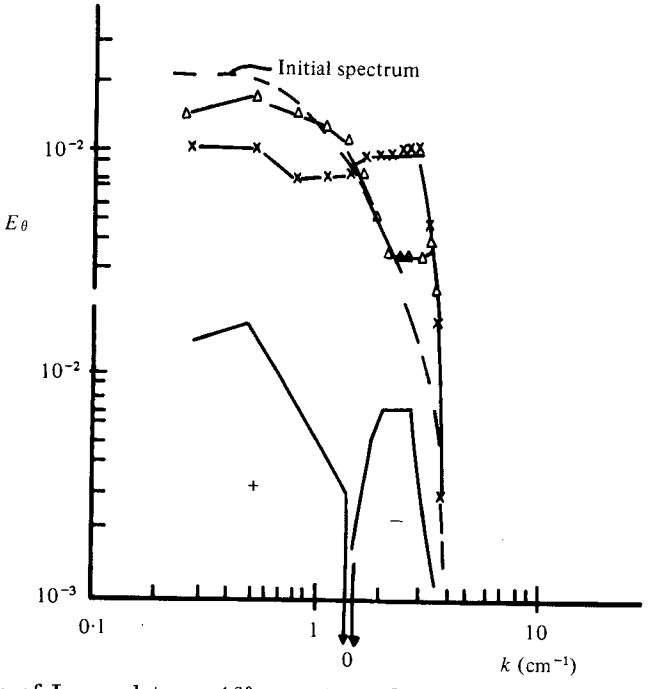

FIGURE 9. Role of Leonard term, 16^3 run, $\Delta_A = h$ = 1·5 cm. Results at 32nd time step: ×, Leonard terms not included; ▽, Leonard term included in temperature field but not in velocity field, ——, Leonard term effect (subtracting × from ▽).

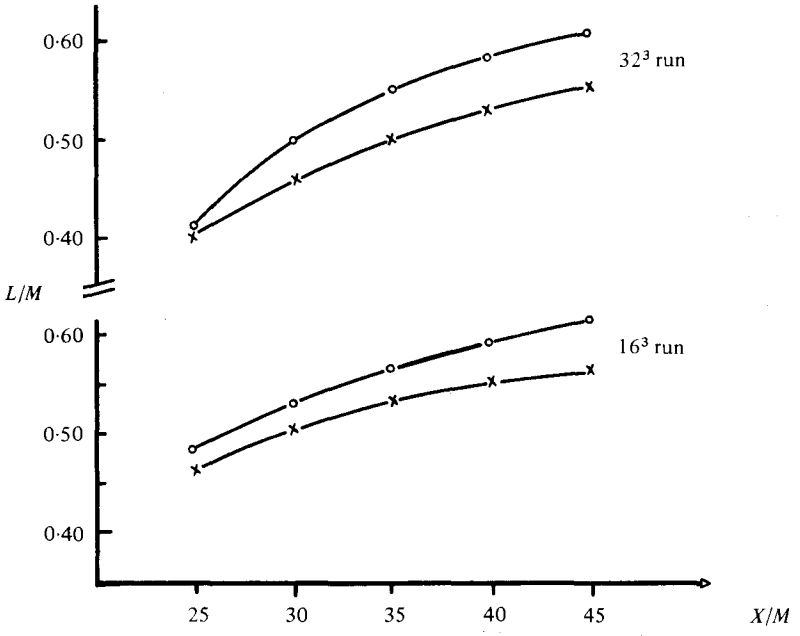

FIGURE 10. Integral scales of velocity $\bar{L}_u$ and temperature $\bar{L}_\theta$. ——, filtered experimental. Simulation: × ×, $\bar{L}_u$; ○ ○, $\bar{L}_\theta$.

Leonard term. It can be seen that this term, instead of draining $\langle\bar{\theta}^2\rangle$ to the SGS, is backscattering $\langle\bar{\theta}^2\rangle$ from the high resolved wavenumbers to the small ones, which is again consistent with the findings for the velocity field.

Finally the thermal diffusivity term effect is investigated: all terms in (3.24), (3.25) were included, apart from the two Leonard terms ($F_{Lu} = F_{L\theta} = 0$). When the molecular viscosity term in (3.24) is included, the effects of the latter are no longer lumped into the subgrid term and a reduction in Cu is necessary ($Cu = 0{\cdot}22$ in this case) to match the kinetic energy decay. Including both, viscosity and thermal diffusivity terms, the value of the parameter C_θ matching the filtered experimental decay of $\langle\bar{\theta}^2\rangle$ was found to be exactly the same, $C_\theta = 2{\cdot}0$. The destruction X_{res} of $\langle\bar{\theta}^2\rangle$ by thermal diffusivity within the resolved scales for a 16^3 run with $h = 15$ mm was found to be

$$\frac{X_{\text{res}}}{X_{\text{total}}} \simeq 6\,\%, \tag{5.13}$$

where X_{total} includes both the drain of $\langle\bar{\theta}^2\rangle$ to subgrid scales and destruction by diffusivity. The ratio $X_{\text{res}}/X_{\text{total}}$ depends on the ratio η_θ/h (η_θ being the Kolmogorov microscale for the temperature field) and it was found approximately the same as the corresponding ratio for the velocity field. This is to be expected for $P_{\mathbf{r}} \simeq 1$. The dissipation range spectrum proposed by Pao (1965) gives

$$\frac{X_k}{X_{\text{total}}} = 1 - \exp\{-1{\cdot}5Ba(k\eta_\theta)^{\frac{4}{3}}\}, \tag{5.14}$$

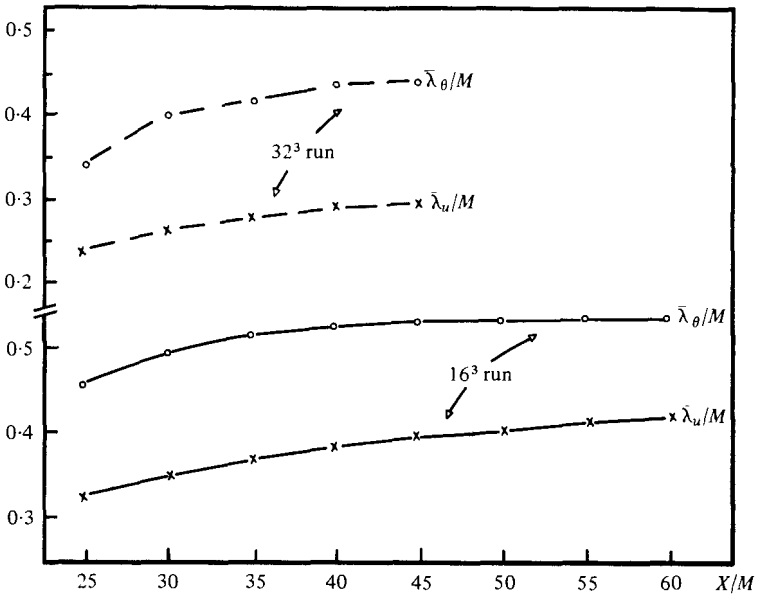

FIGURE 11. Evolution of Taylor microscales. Simulation (M = 4 cm).

where X_k is the destruction of $\langle\theta^2\rangle$ below wavenumber k. Leslie & Quarini (1979) show that a finite-difference scheme on a mesh of width h is equivalent to a sharp cut at wavenumber $2{\cdot}957/h$. Thus Pao's spectrum gives

$$\frac{X_{\text{res}}}{X_{\text{total}}} = 1-\exp\{-6{\cdot}366Ba\,(\eta_\theta/h)^{\frac{4}{3}}\}. \tag{5.15}$$

For the present experiment this gives

$$\frac{X_{\text{res}}}{X_{\text{total}}} \simeq \begin{cases} 6{\cdot}4\,\% & \text{for} \quad Ba = 0{\cdot}63, \\ 8{\cdot}1\,\% & \text{for} \quad Ba = 0{\cdot}83. \end{cases} \tag{5.16}$$

5.3. *Dependence of temperature decay on length scales*

The filtered integral scales, $\bar{L}_u$ for velocity and $\bar{L}_\theta$ for temperature, were computed as

$$\bar{L}_u = \frac{3\pi}{4}\frac{\int_0^\infty k^{-1}\bar{E}_u(k)\,dk}{\int_0^\infty \bar{E}_u(k)\,dk}, \tag{5.17}$$

$$L_\theta = \frac{\pi}{2}\frac{\int_0^\infty k^{-1}\bar{E}_\theta(k)\,dk}{\int_0^\infty \bar{E}_\theta(k)\,dk}, \tag{5.18}$$

and the filtered Taylor microscales as

$$\bar{\lambda}_u^2 = \frac{\langle\bar{u}_1^2\rangle}{\langle(\partial\bar{u}_1/\partial x_1)^2\rangle}, \tag{5.19}$$

$$\bar{\lambda}_\theta^2 = \frac{\langle\bar{\theta}^2\rangle}{\langle(\partial\bar{\theta}/\partial x_1)^2\rangle}. \tag{5.20}$$

Run no.	Initial: Temperature spectrum no. (figures 12*a*, *b*)	k_θ/k_u	λ_u/λ_θ	m	$r = m/n$
0, 1	1	0·33	0·697	0·93	1·05
0, 2	2	0·66	0·74	1·14	1·29
0, 3	3	1·0	0·763	1·25	1·41
0, 4	4	1·33	0·80	1·42	1·61
0, 5	5	1·0	0·77	1·38	1·55

TABLE 1. 16^3 (h = 15 mm) runs with the same initial velocity spectrum (the filtered Yeh & Van Atta spectrum at x/M = 25) and different initial temperature spectra.

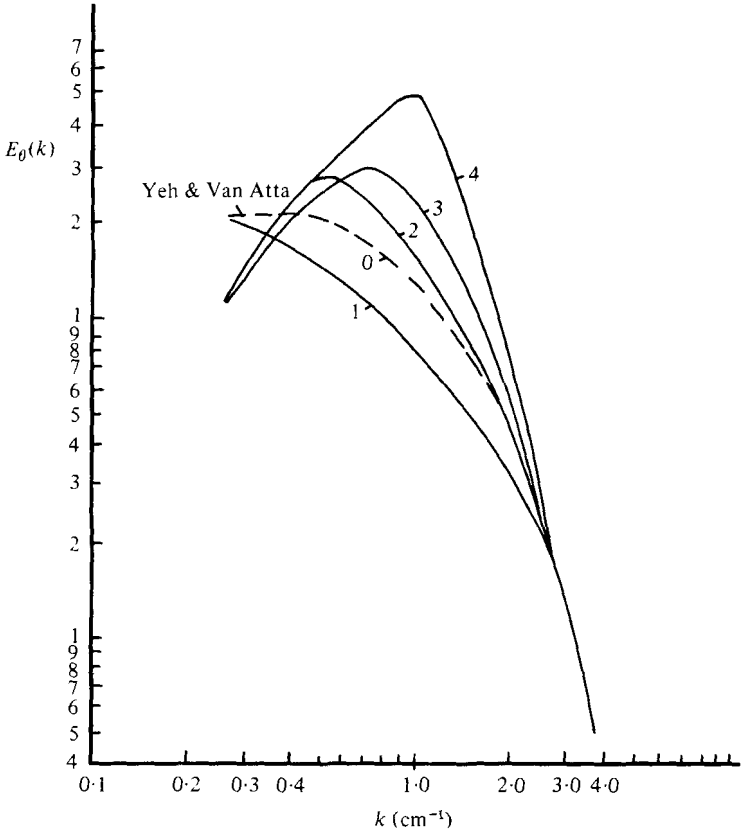

FIGURE 12(*a*). For legend see next page.

Clearly, the scales of the filtered fields must be larger than those of the raw ones. In figure 10 the integral scales obtained from the simulation are compared with the filtered experimental ones; the agreement is excellent, as would be expected from the good agreement on spectra. The evolution of the Taylor microscales is not presented in the Yeh & Van Atta paper; those obtained from the simulation are presented in figure 11.

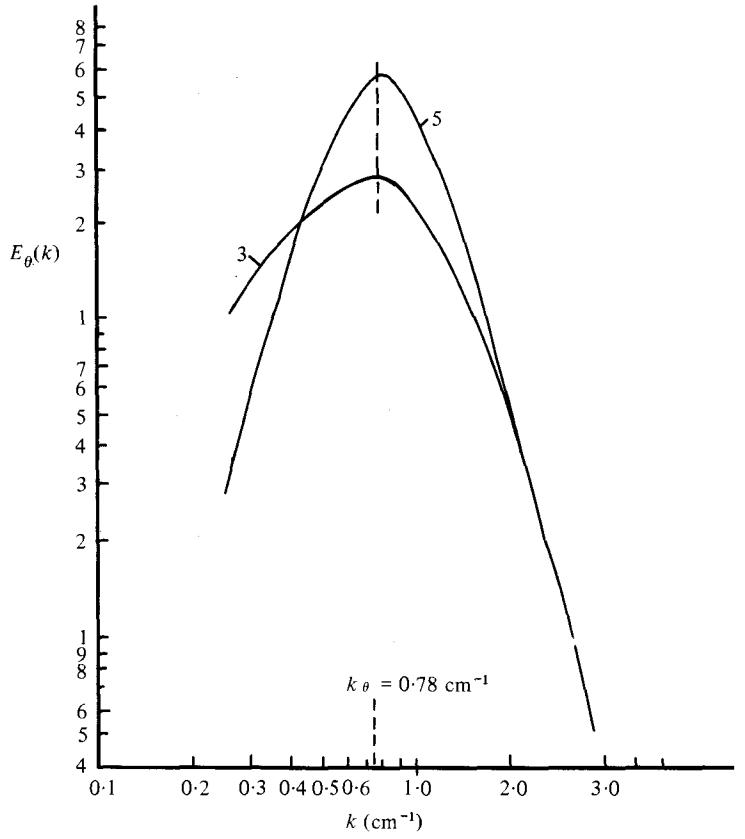

FIGURE 12. (*a*) Shapes of initial three-dimensional temperature spectra used to investigate the dependence of $r = m/n$. 16^3 runs, vertical scale arbitrary. For all initial spectra $\int E_\theta(k)dk$ = const. (*b*) Shapes of initial temperature spectra (3) and (5) both peaking at K_θ = 0·78 cm^{-1}. For both $\int E_\theta(k)\,dk$ = const.

Having established the validity of TEMTY in predicting the statistics of the velocity and temperature fields, the dependence of $r = m/n$ on scales was then investigated. Two sets of runs were carried out; for all of them $\langle \overline{u}_i^2 \rangle$ and $\langle \theta^2 \rangle$ of the initial velocity and temperature fields were those of the Yeh & Van Atta experiment at $x/M = 25$.

In the first set the initial velocity field three-dimensional spectrum was held constant and equal to that of the Yeh & Van Atta experiment at $x/M = 25$, for all runs. A different initial temperature spectrum shape was imposed on each of the five runs. Note that all spectra have, at high wavenumbers, the shape of the Yeh & Van Atta filtered spectrum, i.e. a well-developed inertial–convective range. These are referred to as run numbers 0, 0 to 0, 5; initial data and results are summarized in table 1 and the initial spectral shapes are shown in figure 12.

The values of r so obtained are plotted in figure 13 as a function of k_θ, the wavenumber at which the initial temperature spectrum peaks. Since n and the initial k_u, the wavenumber at which the velocity spectrum peaks, were here constant, this graph may also be viewed as one of m, r *versus* k_θ/k_u.

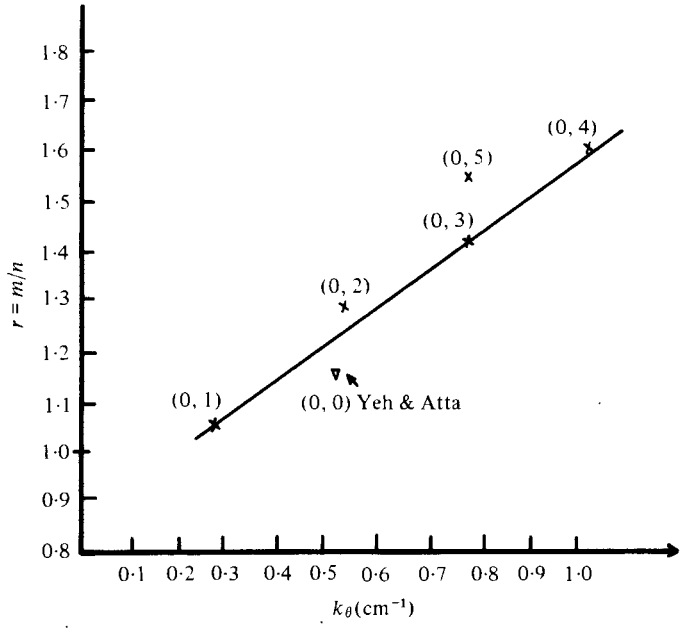

FIGURE 13. $r = m/n$ *versus* initial k_θ; runs (0, 0) to (0, 5). Initial velocity spectrum was the same for all these runs (16^3), that of the Yeh & Van Atta experiment at $X/M = 25$.

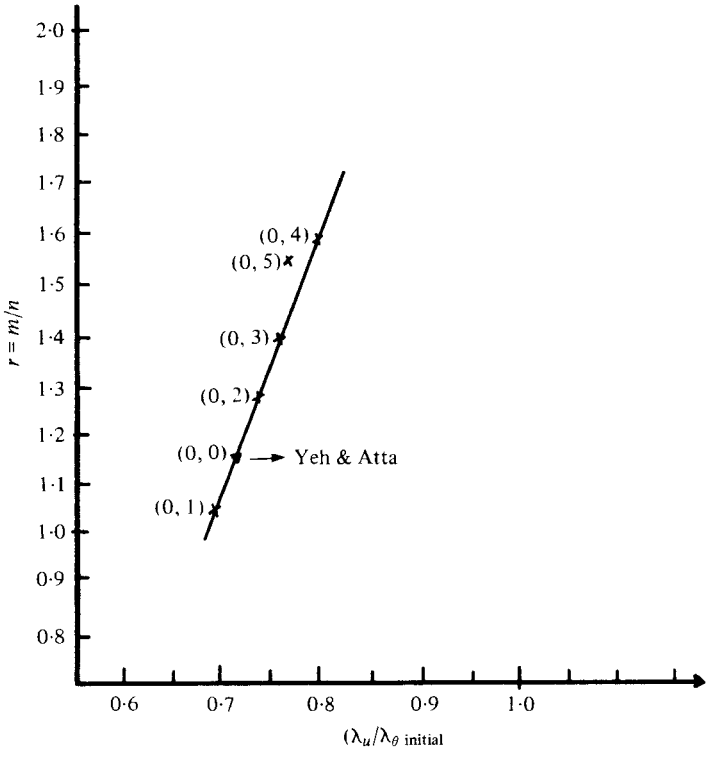

FIGURE 14. $r = m/n$ versus initial $\lambda u/\lambda_\theta$ runs (0, 0) to (0, 5). Initial velocity spectrum for all these runs (16^3) that of the Yeh & Van Atta experiment.

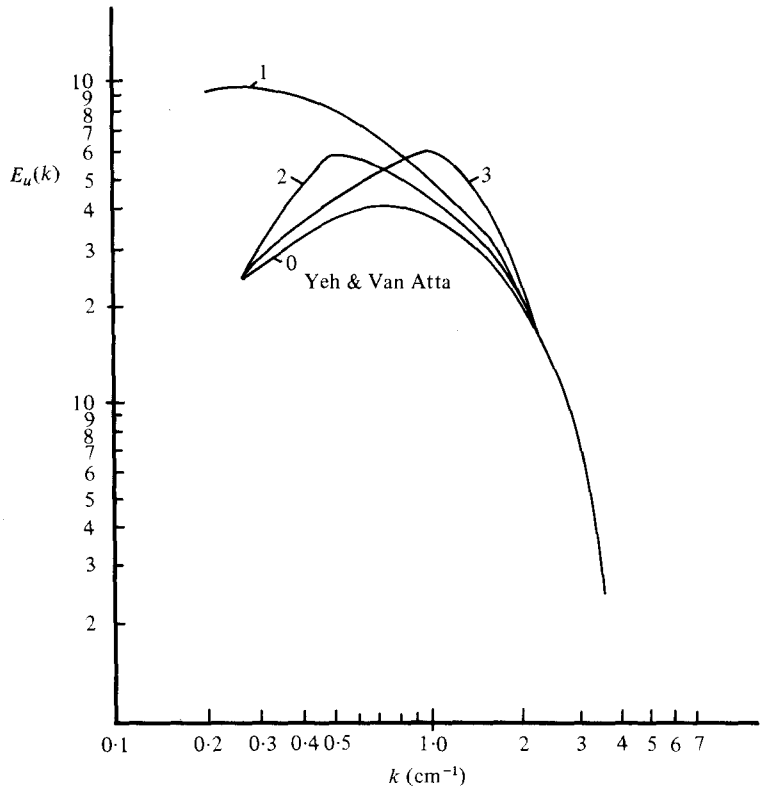

FIGURE 15. Shapes of initial spectra used to investigate the dependence of $r = m/n$. 16^3 runs, vertical scale arbitrary. For all initial spectra, $\int E_u(k)\,dk = \text{const.}$

	Initial				
Run no.	Velocity spectrum no. (figure 13)	Temperature spectrum no. (figure 12)	k_0/k_u	λ_u/λ_θ	$r = m/n$
1, 0	1	0	2·0	0·83	1·66
2, 0	2	0	1·0	0·75	1·28
3, 0	3	0	0·5	0·73	1·14
1, 1	1	1	1·0	0·81	1·51
1, 3	1	3	3·0	0·89	2·01
1, 4	1	4	4·0	0·93	2·29
2, 1	2	1	0·5	0·73	1·17
2, 3	2	3	1·5	0·80	1·57
2, 4	2	4	2·0	0·84	1·79
3, 1	3	1	0·25	0·71	1·03
3, 3	3	3	0·75	0·78	1·39
3, 4	3	4	1·0	0·82	1·59

TABLE 2. 16^3 (h = 15 mm) runs with different initial velocity and temperature spectra.

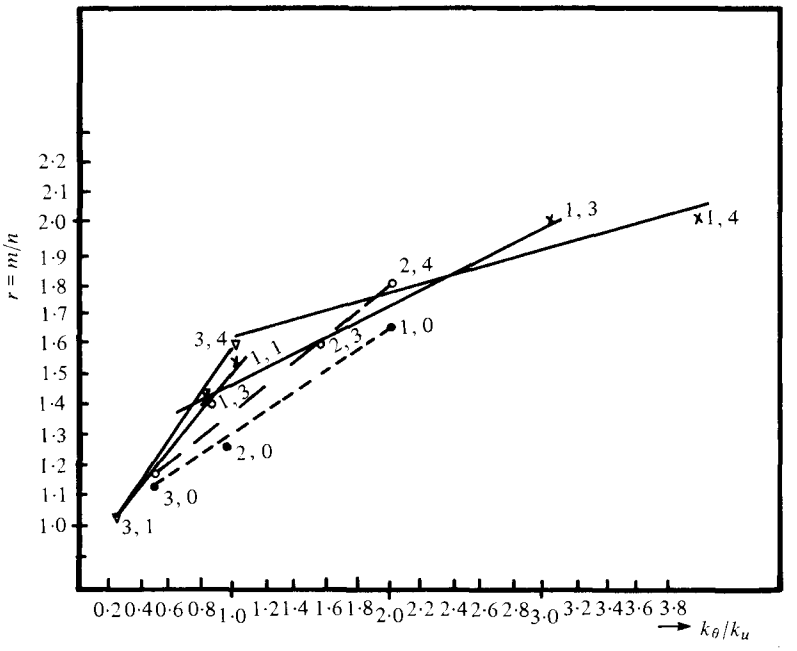

FIGURE 16. $r = m/n$ *versus* k_θ/k_u for different initial velocity and temperature spectra, 16^3 runs.

It can be seen that the results of runs 0, 0 to 0, 4 fall on a straight line in agreement with the Warhaft & Lumley (1978) experiment and the Test Field Model results of Herring & Newman (1979). In fact the set of runs 0,0 to 0,4 is the numerical equivalent of the Warhaft & Lumley experiment.

However, run 0, 5 gives a value of r falling well outside this line; if r was a linear function of k_θ (or k_θ/k_u) the results of runs 0, 3 and 0, 5 should be identical since they both have the same k_θ value. It is seen on figure 12(*b*) that the difference between their initial temperature spectra is at small k's. Although TEMTY reproduces the Warhaft & Lumley experiment it is already clear that m, r are not linear functions of k_θ/k_u. On the other hand when m, r are plotted versus the initial λ_u/λ_θ (figure 14) all points fall on a straight line.

The purpose of the second set of runs was to examine the consequences of varying the initial spectra of the velocity field as well as that of the temperature field. The initial temperature spectra were those of the previous set (figure 12) while the shapes of the initial velocity spectra are shown in figure 15: note that all of these have the same form at high k's. A number of combinations of velocity and temperature spectra were used; the input data and results are summarized in table 2. Anyone run is referred to as run number 1, p, where 1 indicates initial elocity spectrum number and p temperature spectrum number.

The results are plotted in figures 16 and 17. It is clear from figure 16 that r is not a linear function of k_θ/k_u; note though that the r's of runs having either the same first or the second index (i.e. either the same initial velocity or the same initial temperature spectrum) tend to fall on a straight line. On the other hand the results of all runs fall nicely on the same straight line when plotted against λ_u/λ_θ (figure 17) .The spectra of all these runs have the same shape at high wavenumbers.

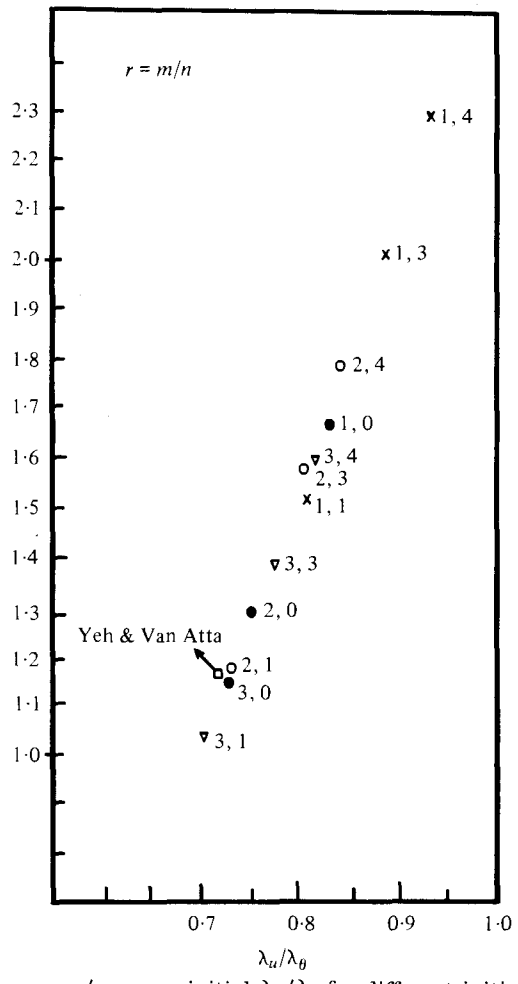

FIGURE 17. $r = m/n$ *versus* initial λ_u/λ_θ for different initial velocity and temperature spectra, 16^3 runs.

We may conclude that the ratio r of the exponents m, n in the decay of the scalar–vector intensities cannot be parametrized by the ratio k_θ/k_u. If there is a well-developed inertial-convective range r is almost perfectly parametrized by the ratio of the length scales λ_u/λ_θ.

6. Conclusions

A LES code (TEMTY) has been developed to calculate the passive scalar in homogeneous isotropic turbulence. The feasibility of LES and the validity of TEMTY has been proven by successful simulation of the Yeh & Van Atta experiment and by the reproduction of the trend observed in the Warhaft & Lumley experiment for the ratio $r = m/n$. The eddy diffusivity subgrid model was found to model correctly the drain of $\langle\overline{\theta}^2\rangle$ to the SGS in the case of isotropic turbulence examined here; the model parameter C_θ was found to be in reasonable agreement with theoretical prediction.

The role of each term in the scalar equation has been investigated; it was shown that, at least for staggered grids, the Leonard term (with its implication of prefiltering) of the scalar equations is not necessary and is, indeed, actively harmful; this term, instead of draining $\langle\overline{\theta}^2\rangle$ to the SGS, backscatters $\langle\overline{\theta}^2\rangle$ from the resolved small scales to the larger ones.

The ratio $r = m/n$ cannot be parametrized by k_θ/k_u; provided there is a well-developed inertial-convective range, an almost perfect linear relationship between r and λ_u/λ_θ was found.

These findings would be rather difficult, expensive and time consuming to arrive at by physical experiments. On the other hand, once the LES code was proven, it was rather inexpensive to change the input parameters at will; this is a clear demonstration of the versatility of LES and its potential in assisting physical understanding, until larger computers make possible the direct application of LES to engineering design problems.

The code TEMTY is an extension of the isotropic velocity field code FORTY, which was developed and tested by Dr M. D. Love, Dr S. T. B. Young and the present author, of the Turbulence Unit, Nuclear Engineering Department, Queen Mary College. The author is grateful to Dr Love and Dr Young and to Professors J. H. Ferziger and D. C. Leslie for many helpful discussions.

Turbulence research in the Department of Nuclear Engineering at Queen Mary College is supported by SRC.

REFERENCES

Antonopoulos-Domis, M. 1979 Aspects of LES of homogeneous isotropic turbulence. *Queen Mary College* EP 6018.

Antonopoulos-Domis, M. & Love, M. D. 1978 The finite difference schemes used in the LES code FORTY. Queen Mary College EP 6032.

Comte-Bellot, G. & Corrsin, S. 1971 Simple Eulerian time correlation of full and narrow band velocity signals in grid generated isotropic turbulence. *J. Fluid Mech.* **48**, 273–337.

Corrsin, S. 1964 Further generalizations of Onsager's cascade model for turbulent spectra. *Phys. Fluids* **7**, 1156.

Ferziger, J. H. & Leslie, D. C. 1979 'Large eddy simulation': a predictive approach to turbulent flow computation. *A.I.A.A. Paper* no. 79/1471.

Herring, J. R. & Newman, G. R. 1979 A test field study of a passive scalar in isotropic turbulence. 2nd Symposium on Turbulence Shear Flows. July 2–4, 1979. Imperial College, London.

Kwak, D., Reynolds, W. C. & Ferziger, J. H. 1975 Three dimensional time dependent computation of turbulent flow. Stanford University Report No. TF-5.

Leonard, A. 1974 Energy cascade in large eddy simulations of turbulent fluid flows. *Adv. Geophys.* A **18**, 237–248.

Leslie, D. C. & Quarini, G. L. 1979 The application of turbulence theory to the formulation of subgrid modelling procedures. *J. Fluid Mech.* **91**, 65–91.

Lilly, D. K. 1966 On the application of the eddy-viscosity concept in the inertial subrange of turbulence. *N.C.A.R.* no. 123.

Lin, S. C. & Lin, S. C. 1973 Study of strong temperature mixing in subsonic grid turbulence. *Phys. Fluids* **16**, 1587–1598.

Mansour, N. N., Moin, P., Reynolds, W. C. & Ferziger, J. H. 1979 Improved methods for large eddy simulations of turbulence. In *Turbulent Shear Flows I*, pp. 386–401. Springer.

Mills, R. R., Kistler, A. L., O'Brien, V. & Corrsin, S. 1958 *N.A.C.A. Tech. Note* no. 4288.

McMillan, O. J. & Ferziger, J. H. 1979 Direct testing of subgrid scale models. *A.I.A.A. Paper* 79-072.

Newman, G. R., Launder, B. E. & Lumley, J. L. 1980 Modelling the behaviour of homogeneous scalar turbulence. *J. Fluid Mech.* (submitted).

Pao, Y. 1965 Structure of turbulent velocity and scalar fields at large wave numbers. *Phys. Fluids* **8**, 1063.

Quarini, G. L. 1977 Applications of closed turbulence theories at high wave numbers, p. 240. Ph.D. thesis, QMC, University of London.

Sepri, P. 1976 Two-point turbulence measurements downstream of a heated grid. *Phys. Fluids* **19**, 1876–1884.

Schuman, U. 1975 Subgrid scale model for finite difference simulations of turbulent flows in plane channels and annuli. *J. Comp. Phys.* **18**, 376–404.

Smagorinsky, J. 1963 General circulation experiments with the primitive equations. *Mon. Weather Rev.* **91** (3), 99–165.

Uberoi, M. S. 1963 Energy transfer in isotropic turbulence. *Phys. Fluids* **6**, 1048.

Van-Atta, C. W. & Chen, W. Y. 1969 Measurements of spectral energy transfer in grid turbulence. *J. Fluid Mech.* **38**, 743.

Warhaft, Z. & Lumley, J. L. 1978 An experimental study of the decay of temperature fluctuations in grid-generated turbulence. *J. Fluid Mech.* **88**, 659–684.

Yeh, T. T. & Van-Atta, C. W. 1973 Spectral transfer of scalar and velocity fields in heated-grid turbulence. *J. Fluid Mech.* **58**, 233–261.